Guidance in Kagome-like photonic crystal fibres II: perturbation theory for a realistic fibre structure

Lei Chen and David M. Bird*

Centre for Photonics and Photonic Materials, Department of Physics, University of Bath, Bath, BA2 7AY, UK

*d.bird@bath.ac.uk

Abstract: A perturbation theory is developed that treats a localised mode embedded within a continuum of states. The method is applied to a model rectangular hollow-core photonic crystal fibre structure, where the basic modes are derived from an ideal, scalar model and the perturbation terms include vector effects and structural difference between the ideal and realistic structures. An expression for the attenuation of the fundamental mode due to interactions with cladding modes is derived, and results are presented for a rectangular photonic crystal fibre structure. Attenuations calculated in this way are in good agreement with numerical simulations. The origin of the guidance in our model structure is explained through this quantitative analysis. Further perspectives are obtained through investigating the influence of fibre parameters on the attenuation.

OCIS codes: (060.2280) Fiber design and fabrication; (060.2400) Fiber properties.

References and links

1. L. Chen, G. J. Pearce, T. A. Birks, and D. M. Bird, "Guidance in Kagome-like photonic crystal fibres I: analysis of an ideal fibre structure," Submitted to Opt. Express (2011).
2. P. W. Anderson, "Localized magnetic states in metals," Phys. Rev. **124**, 41–53 (1961).
3. L. Chen, "Modelling of photonic crystal fibres," Ph.D. thesis, University of Bath (2009).
4. S. Davison and M. Stesliska, *Basic Theory of Surface States* (Oxford U. Press, 1992).
5. E. Economou, *Green's Functions in Quantum Physics* (Springer-Verlag, 1990).
6. F. Couny, F. Benabid, and P. S. Light, "Large-pitch Kagome-structured hollow-core photonic crystal fiber," Opt. Lett. **31**, 3574–3576 (2006).
7. F. Couny, F. Benabid, P. J. Roberts, P. S. Light, and M. G. Raymer, "Generation and Photonic Guidance of Multi-Octave Optical-Frequency Combs," Science **318**, 1118–1121 (2007).
8. A. Argyros and J. Pla, "Hollow-core polymer fibres with a kagome lattice: potential for transmission in the infrared," Opt. Express **15**, 7713–7719 (2007).
9. F. Couny, P. J. Roberts, T. A. Birks, and F. Benabid, "Square-lattice large-pitch hollow-core photonic crystal fiber," Opt. Express **16**, 20626–20636 (2008).
10. N. Guan, S. Habu, K. Takenaga, K. Himeno, and A. Wada, "Boundary element method for analysis of holey optical fibers," J. Lightwave Technol. **21**, 1787–1792 (2003).
11. T.-L. Wu and C.-H. Chao, "Photonic crystal fiber analysis through the vector boundary-element method: effect of elliptical air hole," IEEE Photon. Technol. Lett. **16**, 126–128 (2004).
12. X. Wang, J. Lou, C. Lu, C.-L. Zhao, and W. Ang, "Modeling of pcf with multiple reciprocity boundary element method," Opt. Express **12**, 961–966 (2004).
13. Y. Wang, F. Couny, P. Roberts, and F. Benabid, "Low loss broadband transmission in optimized core-shape kagome hollow-core pcf," in "Lasers and Electro-Optics (CLEO) and Quantum Electronics and Laser Science Conference (QELS), 2010 Conference on," (2010), pp. 1–2.

#141862 - $15.00 USD
Received 27 Jan 2011; accepted 9 Mar 2011; published 25 Mar 2011

1. Introduction

In Ref. [1], an analytic method was developed for an ideal, scalar model of a rectangular hollow-core photonic crystal fibre (PCF). It was found that the fundamental mode is perfectly confined over a wide range of frequencies, providing a baseline from which we aim to explain the broadband guidance observed in a class of Kagome-like PCFs. Our aim in this paper is to extend the analysis of Ref. [1] in order to calculate the attenuation of the fundamental mode in a realistic fibre structure.

For the ideal, scalar model it has been found that a perfectly localised fundamental mode exists both in photonic bands and in bandgaps. With a vector governing equation, we find that the bandgaps vanish and that there are cladding modes with the same propagation constant as the fundamental mode for all frequencies. These cladding modes are glass-guided [1] and have a weak coupling with the fundamental mode owing to the mismatch of the spatial frequencies of the modal fields.

The key point of this work is the use of perturbation theory to include the effects of the vector terms in the governing equation and the structural difference (the high-index intersections) between the ideal and realistic model structures. The method used will need to treat the case of a localised state (the fundamental mode) embedded within a continuum of states (the cladding modes). This problem recalls a case in condensed matter physics. When a localised impurity orbital is embedded in an electron gas, the sharply defined impurity level broadens into a resonance. The width of the resonance is related to the strength of coupling between the localised and continuum states. Anderson [2] analysed this case with the use of Green's function methods and found that the effect of the interaction can be discussed in terms of an imaginary component of the energy of the localised state. This controls the width of the resonance and can be related to the lifetime of an electron initially localised on the impurity. In our case the interaction of the localised and cladding modes has the effect of broadening the fundamental mode into a resonance. The resonance width can be related to an imaginary part of the propagation constant and therefore this leads directly to a measure of the attenuation of the fundamental mode which is caused by the perturbation.

The content of this paper is organised as follows. In Section 2, the perturbation theory is developed to simulate guidance in a realistic model PCF structure. An approximate method to calculate the attenuation due to the interaction of the fundamental and cladding modes is presented. Section 3 gives the results of the perturbation calculations, based on the theory developed in Section 2 and the analysis presented in Ref. [1]. It gives the origin and quantitative explanation of the leakage in our model PCF structure. The effects of the fibre parameters are also investigated. Section 4 is the conclusion.

2. Perturbation theory for the realistic model

2.1. Formulation of perturbation theory for the vector governing equation

We begin our derivation by rewriting the governing equation in a compact form. The scalar governing equation of Eq. (2) in Ref. [1] can be expressed as

$$L^0\mathbf{h}_n = \beta_{0n}^2\mathbf{h}_n, \tag{1}$$

where L^0 denotes $\nabla_t^2 + n_i^2 k_0^2$, and n_i^2 is the dielectric function for the ideal model structure. Here, β_{0n}^2 and $\mathbf{h}_n$ are the eigenvalues and eigenstates of the operator L^0, corresponding to the square of the propagation constants and their associated fields, respectively. The subscript n labels the modes including their polarisation. The vector governing equation corresponding to Eq. (1) in Ref. [1] can be written as

$$L^0\mathbf{H} + \delta L(\mathbf{H}) = \beta^2\mathbf{H}, \tag{2}$$

#141862 - $15.00 USD Received 27 Jan 2011; accepted 9 Mar 2011; published 25 Mar 2011

where the eigenvalue β^2 and eigenvector $\mathbf{H}$ now respectively denote the square of the propagation constant and field for the realistic system. The perturbation term, $\delta L(\mathbf{H})$, is a linear vector function of $\mathbf{H}$. In our particular model structure, $\delta L(\mathbf{H})$ takes the form

$$\delta L(\mathbf{H}) = -\big(\nabla_t \times \mathbf{H}\big) \times \nabla_t \ln n_r^2 + \Delta n^2 k_0^2 \mathbf{H}, \tag{3}$$

where n_r^2 is the dielectric function for the realistic model PCF and $\Delta n^2 = n_r^2 - n_i^2$. Note that this definition of Δn^2 is different from that in Ref. [1]; in this paper Δn^2 is non-zero only at the intersections of the glass strips (where it takes the value $n_a^2 - n_g^2$, where n_a and n_g are refractive indices for air and glass respectively) and is zero elsewhere. The right-hand side of Eq. (3) consists of two parts: the first is the vector term in the governing equation; the second comes from the difference of the dielectric constant between the realistic and ideal model structures. We refer to them as the 'vector term' and 'high-index term', respectively.

The full vector solution $\mathbf{H}$ can be expressed by using the scalar solutions as basis functions: $\mathbf{H} = \sum_n a_n \mathbf{h}_n$, where a_n are expansion coefficients and $\mathbf{H}$ includes $\mathbf{h}_n$ in both the x and y polarisations. Substituting this into Eq. (2) gives

$$L^0\big(\sum_n a_n \mathbf{h}_n\big) + \delta L\big(\sum_n a_n \mathbf{h}_n\big) = \beta^2 \sum_n a_n \mathbf{h}_n. \tag{4}$$

By multiplying $\mathbf{h}_m^*$ on both sides of Eq. (4) and using the ortho-normalisation formula $\int\int \mathbf{h}_m^* \cdot \mathbf{h}_n dA = \delta_{mn}$ within one supercell, we find

$$\sum_n (L_{mn}^0 + \delta L_{mn}) a_n = \beta^2 a_m, \tag{5}$$

where

$$L_{mn}^0 = \delta_{mn} \beta_{0m}^2 \tag{6}$$

and

$$\delta L_{mn} = \int\int \mathbf{h}_m^* \cdot \delta L(\mathbf{h}_n)\, dA. \tag{7}$$

Equation (5) is a perturbation matrix equation, where interactions between modes of the ideal, scalar structure are expressed via the matrix elements. Substituting Eq. (3) into Eq. (6), the vector and high-index perturbation terms respectively become

$$\delta L_{mn}^a = -\int\int \mathbf{h}_m \cdot \left[\big(\nabla_t \times (\mathbf{h}_n)\big) \times \nabla_t \ln n_r^2\right] dA \tag{8}$$

and

$$\delta L_{mn}^b = \int\int \mathbf{h}_m \cdot (\Delta n^2 k_0^2) \mathbf{h}_n \, dA. \tag{9}$$

The integrals are over one supercell, but in practice the integral in Eq. (9) is only over the intersections of the glass strips.

In Ref. [1], the fields $\mathbf{h}_m$ and $\mathbf{h}_n$ have been analytically expressed using trigonometric functions. Moreover, the separation of the scalar fields along the x and y axes reduces the area integrals in Eqs. (8) and (9) to one dimensional integrals. This makes the calculation of the matrix elements very straightforward and efficient. The details of the derivation are provided in Ref. [3].

The perturbation terms δL_{mn} in Eq. (5) can be classified into three types. The first are diagonal elements δL_{mm}. These terms can be included in L^0 and cause a shift of the propagation constant for each mode. However, this effect does not lead to any interaction with other modes and therefore does not contribute to the loss. The diagonal terms of Eq. (5) can be rewritten as

$$L_{mm}^0 + \delta L_{mm} = \beta_{0m}'^2, \tag{10}$$

#141862 - $15.00 USD Received 27 Jan 2011; accepted 9 Mar 2011; published 25 Mar 2011

where β'_{0m} is the shifted propagation constant of the mode m, including both vector and high-index terms. As we shall see, these diagonal terms are substantially larger than the off-diagonal matrix elements. When considering cladding modes that have propagation constants close to the fundamental mode, it is these shifted eigenvalues that will be analysed. It is also these shifts that remove the bandgaps that are present in a scalar solution of the ideal model structure.

The second type of matrix element, $\delta L'_{mn}$, contains $\delta L_{m_0 n}$ and $\delta L_{n m_0}$, where m_0 denotes m_{0x} or m_{0y}, representing the x or y polarised fundamental mode, and n labels a cladding mode. Coupling of this type leads to light leaking from the fundamental mode into the cladding, giving rise to confinement loss. The third type, $\delta L''_{mn}$, represents interactions between different cladding modes. In principle these is a fourth type of matrix element $\delta L_{m_{0x} m_{0y}}$ and $\delta L_{m_{0y} m_{0x}}$ which represent coupling between the two polarisations of the fundamental mode. In practice, however, these terms are zero due to symmetry.

2.2. Attenuation due to mode interactions

If we solve Eq. (5) directly this gives only a real propagation constant and therefore can not address attenuation. We therefore will use a Green's function method from which attenuation can be derived. As mentioned in the introduction, this is similar to the problem for an impurity embedded in an electron gas; in our case the fundamental mode is the 'impurity' and the continuum of cladding modes is the 'electron gas'. We follow Anderson's method [2], extending this to include vector effects. It is important to note that an analytic treatment is impossible if all the perturbation terms are considered. If, however, we neglect the interaction terms $\delta L''$ between different cladding modes, an analytic analysis can be performed. This approximation should be applicable because the attenuation is mainly caused by the interaction between the fundamental mode and cladding modes. The cladding-cladding terms are likely to be less important in affecting the overall magnitude of the attenuation.

In the following derivation, we focus on the x polarised fundamental mode; the expressions for the y polarisation are equivalent. Having dropped the $\delta L''$ terms from Eq. (5), the Green's function is defined by

$$\sum_{v} (L^0_{mm}\delta_{mv} + \delta L_{mm}\delta_{mv} + \delta L'_{mv}) G_{vn} = -\delta_{mn}. \tag{11}$$

The equivalent diagonal Green's function is defined by

$$(L^0_{mm} + \delta L_{mm}) G^0_{mm} = -1, \tag{12}$$

and can be written as

$$G^0_{mm} = \left(\beta^2 - \beta'^2_{0m} + i\varepsilon\right)^{-1}, \tag{13}$$

where ε approaches zero from below. The two Green's operators in Eqs. (11) and (12) are related by the Dyson equation [4]

$$G_{ab} = G^0_{aa}\delta_{ab} + \sum_{p,q} G^0_{ap}\delta L'_{pq} G_{qb}, \tag{14}$$

where we note that for $\delta L'_{pq}$ to be non-zero, either p or q must label a fundamental mode. When the subscripts $\{ab\}$ of G_{ab} are chosen as $\{m_{0x}m_{0x}\}$, $\{m_{0y}m_{0x}\}$ and $\{mm_{0x}\}$, Eq. (14) becomes

$$G_{m_{0x}m_{0x}} = G^0_{m_{0x}m_{0x}} + G^0_{m_{0x}m_{0x}} \sum_{m} \delta L'_{m_{0x}m} G_{mm_{0x}}, \tag{15}$$

$$G_{m_{0y}m_{0x}} = G^0_{m_{0y}m_{0y}} \sum_{m} \delta L'_{m_{0y}m} G_{mm_{0x}}, \tag{16}$$

#141862 - $15.00 USD Received 27 Jan 2011; accepted 9 Mar 2011; published 25 Mar 2011

and

$$G_{mm_{0x}} = G^0_{mm}\delta L'_{mm_{0x}}G_{m_{0x}m_{0x}} + G^0_{mm}\delta L'_{mm_{0y}}G_{m_{0y}m_{0x}}, \tag{17}$$

where we note that m labels cladding modes only. Substituting Eq. (17) into Eqs. (15) and (16), we obtain

$$G_{m_{0x}m_{0x}} = G^0_{m_{0x}m_{0x}} + G^0_{m_{0x}m_{0x}}G_{m_{0x}m_{0x}}V_{m_{0x}m_{0x}} + G^0_{m_{0x}m_{0x}}G_{m_{0y}m_{0x}}V_{m_{0x}m_{0y}}, \tag{18}$$

and

$$G_{m_{0y}m_{0x}} = \frac{G^0_{m_{0y}m_{0y}}G_{m_{0x}m_{0x}}V_{m_{0y}m_{0x}}}{1 - G^0_{m_{0y}m_{0y}}V_{m_{0y}m_{0y}}}, \tag{19}$$

where $V_{ab} = \sum_m \delta L'_{am}G^0_{mm}\delta L'_{mb}$; by using Eq. (13) it can be written as

$$V_{ab} = \sum_m \frac{\delta L'_{am}\delta L'_{mb}}{\beta^2 - \beta'^2_{0m} + i\varepsilon}. \tag{20}$$

Substituting Eq. (19) into Eq. (18), we obtain an expression for $G_{m_{0x}m_{0x}}$:

$$G_{m_{0x}m_{0x}} = \frac{G^0_{m_{0x}m_{0x}}}{1 - G^0_{m_{0x}m_{0x}}V_{m_{0x}m_{0X}} - \frac{G^0_{m_{0x}m_{0x}}G^0_{m_{0y}m_{0y}}V_{m_{0x}m_{0y}}V_{m_{0y}m_{0x}}}{1-G^0_{m_{0y}m_{0y}}V_{m_{0y}m_{0y}}}}. \tag{21}$$

Because of the symmetry of the two polarised fundamental modes, we have $G^0_{m_{0x}m_{0x}} = G^0_{m_{0y}m_{0y}}$; we also note that $V_{m_{0x}m_{0x}} = V_{m_{0y}m_{0y}}$ and $V_{m_{0x}m_{0y}} = V_{m_{0y}m_{0x}}$. Equation (21) then becomes

$$G_{m_{0x}m_{0x}} = \left((G^0_{m_{0x}m_{0x}})^{-1} - V_{m_{0x}m_{0x}} - \frac{V^2_{m_{0x}m_{0y}}}{(G^0_{m_{0x}m_{0x}})^{-1} - V_{m_{0x}m_{0x}}} \right)^{-1}. \tag{22}$$

In Eq. (22), the term containing $V^2_{m_{0x}m_{0y}}$ can be neglected because, as discussed below, the magnitude of the matrix elements is small. Equations (13), (20), and (22) are then combined to give

$$G_{m_{0x}m_{0x}} = \left(\beta^2 - \beta'^2_{0m_{0x}} + i\varepsilon - \sum_m \frac{\delta L'_{m_{0x}m}\delta L'_{mm_{0x}}}{\beta^2 - \beta'^2_{0m} + i\varepsilon} \right)^{-1}, \tag{23}$$

where $\beta'_{0m_{0x}}$ is determined by Eq. (10) and denotes the shifted propagation constant of the x polarised fundamental mode.

By comparing Eqs. (13) and (23), it can been seen that the perturbation term in Eq. (23) acts as an additional shift in the square of the propagation constant of the fundamental mode, arising from the interaction with the cladding modes. It is important to note that this perturbation term is complex. The real part is relatively unimportant (causing a small shift in the propagation constant), but the existence of an imaginary part leads directly to an attenuation of the fundamental guided mode. By using the identity [5]

$$\lim_{y\to 0} \frac{1}{x + iy} = P\frac{1}{x} - i\pi\delta(x), \tag{24}$$

where P is the principal value and $\delta(x)$ is a Dirac delta function, the imaginary part of the perturbation terms in Eq. (23) can be expressed as

$$\Delta\beta^2_{m_{0x}[Imag]} = \pi\sum_m \delta L'_{m_{0x}m}\delta L'_{mm_{0x}}\delta\left(\beta^2 - \beta'^2_{0m}\right). \tag{25}$$

#141862 - $15.00 USD Received 27 Jan 2011; accepted 9 Mar 2011; published 25 Mar 2011

Equation (25) is the key equation of this paper; it gives an analytic expression from which the attenuation of the fundamental mode due to interaction with cladding modes can be derived. It can be seen that the attenuation depends on two factors. One is the density of the cladding states which is expressed through the term $\sum_m \delta\left(\beta^2 - \beta_{0m}'^2\right)$; the second is the perturbation matrix elements $\delta L'_{m_{0x}m}\delta L'_{mm_{0x}}$, where m_{0x} and m are labels of the x polarised fundamental mode and cladding modes, respectively. The values of both of these parts can be calculated using Eqs. (8) to (10).

To complete our analysis of the attenuation we write

$$\beta^2_{m_{0x}[Cmplx]} = \beta'^2_{0m_{0x}[Real]} + i\Delta\beta^2_{m_{0x}[Imag]}. \tag{26}$$

To first-order, the imaginary part of the propagation constant is then given by

$$\beta_{m_{0x}[Imag]} = \Delta\beta^2_{m_{0x}[Imag]}/(2\beta'_{0m_{0x}[Real]}). \tag{27}$$

In a practical calculation of the attenuation, the Delta function in Eq. (25) needs to be broadened. We use a Gaussian smoothing, and Eq. (25) then becomes

$$\Delta\beta^2_{m_{0x}[Imag]} = \pi\sum_m \frac{1}{\sqrt{2\pi}\sigma}\exp\left\{-\frac{\left[\left(\beta^2-\beta_{0m}'^2\right)/\sigma\right]^2}{2}\right\}\delta L'_{m_{0x}m}\delta L'_{mm_{0x}}, \tag{28}$$

where $1/\sigma\sqrt{2\pi}$ is a normalisation factor. The width corresponding to each mode is controlled by σ; a small value of σ represents slight smoothing and a sharp peak in the plots. The value of σ will be determined through convergence tests in the following.

3. Results for the model PCF structure

3.1. Mode distribution and interaction

As discussed in Ref. [1], the model rectangular hollow-core PCF has a square cladding lattice, and the central defect is created by moving outward the four glass strips that enclose the central square air hole. We use a 'standard' structure in which the thickness of the glass strips and the shift to create the central defect are set at 0.05Λ and 0.125Λ, respectively. In the remainder of this paper, all quantities will be made dimensionless by using the pitch Λ of the cladding lattice as the unit of length. We therefore use $(\beta\Lambda)^2$ for the dimensionless propagation constant and $\delta L'\Lambda^2$ for the dimensionless perturbation matrix element.

Our investigation focuses on the cladding modes close to the air-line. In the previous paper, scalar modes have been calculated for an ideal model structure which has a higher refractive index at the intersections of the glass strips [1]. Solutions for the vector governing equation and for the realistic structure (without the high-index intersections) have a shifted value of $(\beta\Lambda)^2$, which is determined by Eq. (10). These shifted modes are the basis states for our perturbation theory. We calculate the diagonal shift for all the scalar modes of the ideal structure and then consider only the shifted modes which are close to the air-line in the calculation of attenuation.

We start by considering an 8×8 supercell with a normalised frequency $k_0\Lambda = 40$; this was analysed in detail in Ref. [1]. The calculation of the diagonal shift gives 64 basis states which are air-guided modes (including the fundamental mode) and 48 basis states which are glass-guided modes, that are located in the vicinity of the fundamental mode (within a distance of $(\beta\Lambda)^2$ less than 20). After the diagonal shift, the $(\beta\Lambda)^2$ value for the fundamental guided mode is 1587.463, which is 0.342 greater than the unperturbed value. The nearest air-guided and glass-guided modes are separated from the fundamental mode by $(\beta\Lambda)^2$ differences of 1.905 and 0.199, respectively.

#141862 - $15.00 USD Received 27 Jan 2011; accepted 9 Mar 2011; published 25 Mar 2011

From Eqs. (8) and (9), the vector and high-index perturbation matrix elements can be calculated. For the vector terms, the average diagonal shifts of $(\beta\Lambda)^2$ are 0.604 and 222.707 for the air-guided and glass-guided modes, respectively. By comparison, the off-diagonal elements of the vector term are considerably smaller. Typical values are of order 10^{-1}, 10^0 and 10^{-3} respectively for air-air, glass-glass and air-glass interactions for the same polarised modes. For the interaction between different polarisations, they are of order 10^{-5}, 10^0 and 10^{-2} for the three groups. The high-index terms exhibit a rather different pattern. The average diagonal shifts are 0.001 and 32.705 for the air-guided and glass-guided modes, which are significantly smaller than for the vector term. For the off-diagonal elements of high-index term, typical values are 10^{-5}, 10^0 and 10^{-2} for air-air, glass-glass and air-glass mode interactions with the same polarisation; the interactions between differently polarised modes are identically zero. In general, we conclude that, apart from the diagonal term, the magnitude of the perturbation is relatively small, which gives us confidence in the validity of our perturbation theory. This also justifies our neglect of the second order terms in Eq. (22). In general the vector terms tend to be larger than the high-index terms, but neither can be neglected in the perturbation calculation.

3.2. Attenuation calculations

In order to use Eqs. (27) and (28) to calculate the attenuation, both the size of supercell and an appropriate σ value should first be determined. For high precision, we want σ sufficiently small so that only those states close to the fundamental mode are included. However, we also need an adequate number of these cladding states for computational accuracy. In this case, the size of supercell should be as large as possible. However, a problem arises if the supercell becomes too large. As discussed in the previous paper, modes are found by searching for identical field values at the centres of neighbouring supercells [1]. When the size of supercell is enlarged, the transfer matrices must pass through more air and glass layers. For some modes, the fields are confined only within a subset of layers and decay exponentially in others. To find these modes in a large supercell requires very high floating-point accuracy. For supercells exceeding 32×32 in size, even quadruple precision is insufficient. In the determination of σ values, we have therefore chosen a set of supercells no larger than 32×32.

Since our investigation concerns the properties of the fundamental mode, the $(\beta\Lambda)^2$ value on the right-hand side of Eq. (28) should be chosen to be that of the fundamental mode. However, to investigate convergence of the calculations it is convenient to plot the imaginary part of $\Delta(\beta\Lambda)^2$ for the fundamental mode as a function of $(\beta\Lambda)^2$. In general, we find that the air-guided modes have much higher density of states than the glass-guided modes; we therefore consider the air-guided and glass-guided modes separately. A larger σ is required for the glass-guided modes to give a smooth density of states. Plots of the imaginary part of $\Delta(\beta\Lambda)^2$ for the fundamental mode are shown in Fig. 1 as a function of the smoothing width σ and the size of the supercell.

For the air-guided modes, we find that the smallest value of σ that provides well converged results is 0.3. In this case the difference between 28×28 and 32×32 supercells is less than 1% over the whole range shown in Fig. 1. The glass-guided modes show a broader distribution over a wide range of $(\beta\Lambda)^2$, as shown in the right of Fig. 1. It is found that the smallest acceptable value of σ is 10 for the largest supercell we have used. In this case the difference between 28×28 and 32×32 supercells is less than 2% over the range shown in Fig. 1.

Figure 1 shows an important result that the imaginary part of $\Delta(\beta\Lambda)^2$ at the propagation constant of the fundamental guided mode is non-zero only for the glass-guided modes. The density of states of air-guided modes is zero at this propagation constant and so these modes do not contribute to the attenuation. We conclude that interaction with the glass-guided modes determines attenuation in the high-transmission region. This should also be valid for other members of the

#141862 - $15.00 USD Received 27 Jan 2011; accepted 9 Mar 2011; published 25 Mar 2011

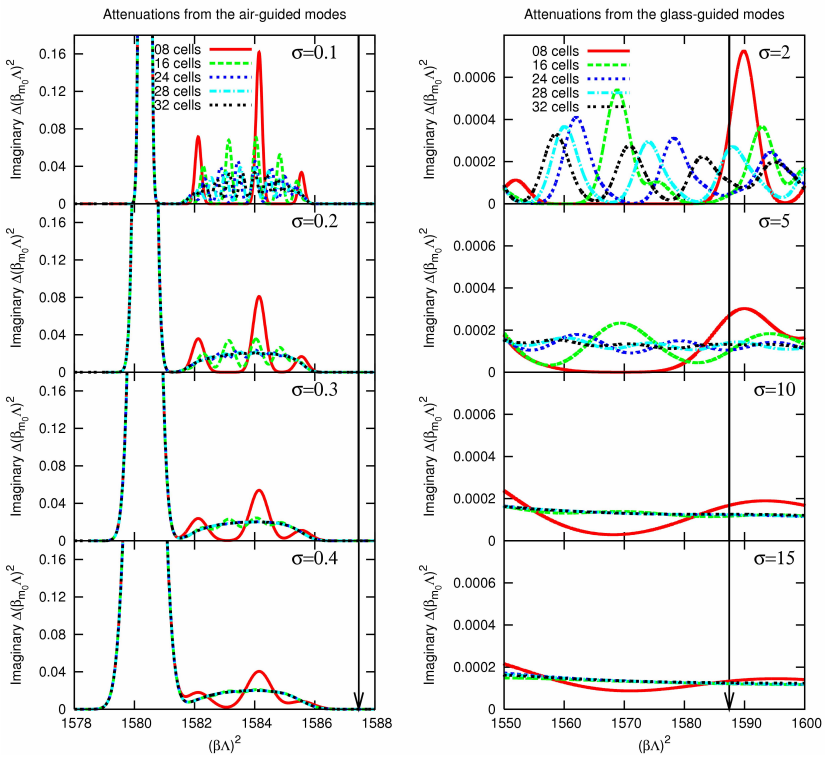

Fig. 1. Variation of the imaginary part of $\Delta(\beta\Lambda)^2$ for the fundamental mode with smoothing width σ for different sizes of supercells calculated using Eq. (28). The left and right panels show contributions from air-guided and glass-guided cladding modes, respectively. The black arrows at $(\beta\Lambda)^2 = 1587.463$ indicate the location of the shifted fundamental guided mode.

class of PCFs that guide light due to weak coupling of modes, and thus provides quantitative support for the conclusions drawn for Kagome [6–8] and square-lattice [9] hollow-core PCFs.

3.3. Frequency dependence of the attenuation

Having developed a method to calculate the imaginary part of β, we now use it to analyse the dependence of the attenuation on frequency and fibre structure. At the sample frequency of $k_0\Lambda = 40$, the imaginary part of $\beta\Lambda$ for the fundamental mode is calculated to be 1.58×10^{-6}, indicating a low level of leakage.

Figure 2(a) shows the attenuation over a range of normalised frequencies from $k_0\Lambda = 26$ to 46 at a spacing of 0.2. Similar to that observed in Kagome and square-lattice hollow-core PCFs, the attenuation for rectangular hollow-core PCFs varies dramatically as a function of frequency. In the selected range, it generally shows a decreasing trend with increasing frequency. This feature can also be seen via three peaks at $k_0\Lambda = 28.0$, 33.2 and 37.4, for which the imaginary $\beta\Lambda$ declines from 5.1×10^{-5} to 1.3×10^{-5}.

To test the validity of our perturbation calculation we have used the boundary element method [10–12] to calculate the attenuation. We use a model rectangular hollow-core PCF, a schematic of the fibre structure is shown in the inset of Fig. 2(a). All the structural parameters are the same as those used in the perturbation calculations, except for the details at the edge of the

#141862 - $15.00 USD Received 27 Jan 2011; accepted 9 Mar 2011; published 25 Mar 2011

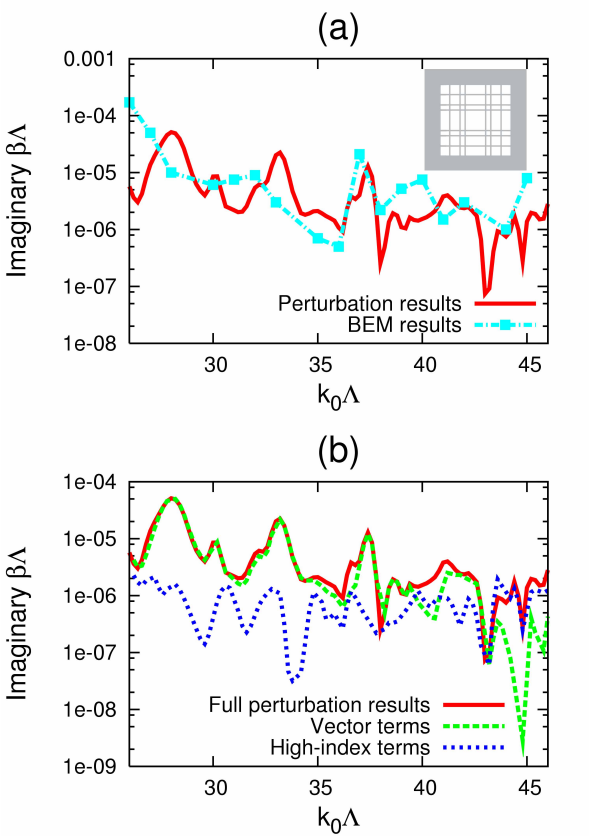

Fig. 2. Imaginary part of the propagation constant of the fundamental mode over a range of frequencies in the first transmission window. (a) Comparison between perturbation and boundary element methods. The inset shows the schematic model PCF structure calculated by the boundary element method. (b) The effect of the perturbation terms, where the red line indicates the full perturbation result; the green and blue lines are results that include only the vector and high-index perturbation terms, respectively.

cladding, where the boundary element method requires an enclosed glass jacket rather than a supercell geometry. Details of the boundary element calculations are given in Ref. [3]. The comparison in Fig. 2(a) shows that results for the attenuation are in good agreement in their order of magnitude and they exhibit a similar variation with frequency. Although the details do not match well, this is to be expected because the calculated structures are not identical. Leakages for Kagome and square-lattice hollow-core PCFs were measured experimentally in the same high-transmission window, although the resonance frequencies differ because of the fibre structures. In these experiments, the confinement losses varied from about 0.5 dB/m to 1.5 dB/m in Kagome PCFs (with pitch Λ=10.9 μm) [6], and from 1 dB/m to 4 dB/m in square-lattice hollow-core PCFs (with pitch $\Lambda = 17\mu$m) [9] over a continuous range of frequencies. In our model structure, the typical level of the imaginary part of $\beta\Lambda$ is between 10^{-6} and 10^{-5}. The corresponding confinement loss varies from 0.58 dB/m to 5.8 dB/m (if we choose the pitch $\Lambda = 15\mu$m), in good agreement with the experimentally measured values.

Figure 2(b) shows the separate attenuations calculated using only the vector or high-index perturbation terms. This comparison shows that the vector terms are the dominant effect in the

#141862 - $15.00 USD
Received 27 Jan 2011; accepted 9 Mar 2011; published 25 Mar 2011

attenuation, including the high-loss peaks. The influence of the high-index terms remains at a relatively low level, and only for the lowest losses is their effect comparable to that of the vector terms. This feature indicates that the coupling of the modes arising from the air-glass interface in much more significant than that from the intersections of the glass strips.

For frequencies close to a resonance of the glass strips, the confinement loss of PCFs significantly increases [7, 8]. Assuming that the fundamental guided mode is located on the air-line, i.e. $\beta = k_0$, the resonance condition is given by $k_0\Lambda\sqrt{n_g^2 - n_a^2}\cdot t/\Lambda = j\pi$ [7], where n_g and n_a are the refractive indices for the glass and air, respectively, t is the thickness of the glass strips, and j is an integer. In the vicinity of a resonance the attenuation is found to increase; in Kagome hollow-core PCFs, a high loss region of width 200 nm separates the high transmission windows [7]. In our model structure, the value of t/Λ is 0.05; the lowest normalised resonance frequency is therefore $k_0\Lambda = 56.2$. The attenuations shown in Fig. 2 are located within the first high-transmission window (i.e. between $j = 0$ and 1). In the following calculations, we focus on the guidance only within this window.

Near to the resonance frequency, our calculated attenuation values become negative and therefore unphysical. In this case, the choice of considering only the glass-guided modes is not sufficient to calculate the attenuation. A number of modes are located very close to the fundamental guided mode. Their fields occupy both the air and the glass regions, showing that they are 'precursors' to the set of higher-order glass-guided modes that are about to be trapped. These characteristics lead to a strong coupling with the fundamental guided mode, giving rise to contributions to attenuation that are not included in our model.

3.4. Effect of the fibre structure

The confinement loss can also be calculated as a function of the thickness of the glass strips. In this investigation, the centres of each air and glass region are unchanged, and the thicknesses of all the glass strips are kept the same.

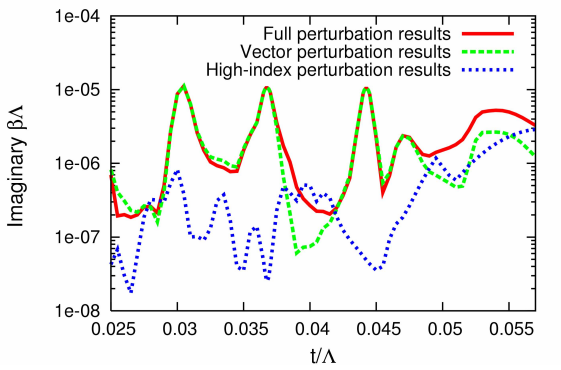

Fig. 3. Imaginary part of the propagation constant as a function of the glass strip thickness in the first transmission window when $k_0\Lambda = 40$. The full, vector and high-index perturbation results are shown in red, green and blue, respectively.

Figure 3 shows the attenuation of the fundamental guided mode versus the thickness of the glass strips at $k_0\Lambda = 40$. Similar peaks to those observed in Fig. 2 appear at $t/\Lambda = 0.030$, 0.037 and 0.044; a comparison between the two plots shows that reducing the thickness of the glass struts leads to a shift of the attenuation feature towards a lower wavelength. For example, the highest frequency peak for $t/\Lambda = 0.05$ is at $k_0\Lambda = 37.4$; for the structure with $t/\Lambda = 0.044$, it moves to $k_0\Lambda = 40.0$. However, the overall appearance of the attenuation features remains

#141862 - $15.00 USD Received 27 Jan 2011; accepted 9 Mar 2011; published 25 Mar 2011

unchanged.

We now consider the effect of the size of the central defect; the full width of the central air hole is labelled D. The frequency $k_0\Lambda$ and the thickness of glass strips t/Λ are fixed at 40 and 0.05, respectively. The central defect is made by simultaneously moving the four glass strips nearest to the centre by a distance of between 0.03Λ and 0.185Λ.

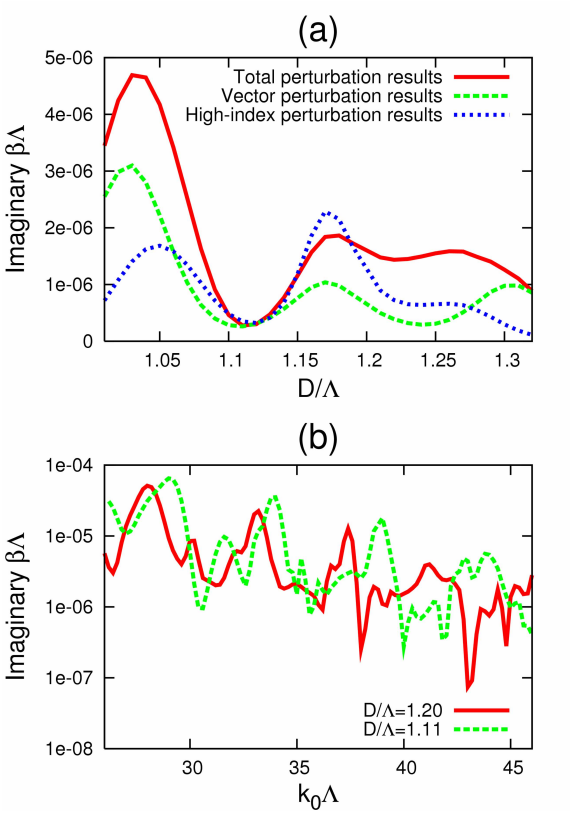

Fig. 4. (a) Dependence of attenuation on the size of the central defect. Full, vector and high-index perturbation results are shown in red, green and blue, respectively. (b) Attenuations for the two sizes of central defect as a function of frequency. The red and green lines respectively correspond to $D = 1.20\Lambda$ and $D = 1.11\Lambda$.

Figure 4(a) presents attenuations for different sizes of central defect. The values of the imaginary $\beta\Lambda$ vary more smoothly than those for the strut thickness, from 2.7×10^{-7} to 4.7×10^{-6}. The plots show a low-attenuation region, from $D = 1.1\Lambda$ to 1.15Λ, surrounded by two relatively high-loss areas. The minimum value of the imaginary $\beta\Lambda$ is about 2.8×10^{-7} (i.e. a loss of 0.16 dB/m for $\Lambda = 15\mu$m) at 1.11Λ. In this case, both the vector and the high-index perturbations are simultaneously suppressed.

For a more detailed view of this low-loss region, the attenuation for a central defect size of 1.11Λ has been plotted as a function of frequency. The results in Fig. 4(b) show a comparison of the attenuation with the formerly used central defect of $D = 1.20\Lambda$. They exhibit a very similar variation with frequency, but for the smaller core size, the attenuation characteristic is shifted towards a lower wavelength. This is similar to what happens for the thinner glass strips. A comparison of the magnitude in Fig. 4(b) shows that, for a larger central defect, the average value of the leakage is relatively smaller.

#141862 - $15.00 USD
Received 27 Jan 2011; accepted 9 Mar 2011; published 25 Mar 2011

4. Conclusion

The key technical development of this study is the finding that a perturbation method is effective in the investigation of a class of PCFs which govern light due to the weak coupling of the fundamental mode and cladding modes. We have derived an expression for the attenuation which allows for rapid calculations and which is in good agreement with large-scale numerical calculations.

Our quantitative analysis for rectangular hollow-core PCFs has shown that the fibre leakage arises from the interaction between the fundamental mode and the cladding modes, and physically relates to the density of states of the cladding modes weighted by the magnitude of their coupling with the fundamental mode. In high-transmission windows, the contribution of the air-guided modes to attenuation is found to be very small. Although the glass-guided modes may closely match the fundamental mode in terms of their propagation constants, the large difference in the spatial frequencies of their fields greatly suppresses the leakage of light.

In our model structure, a smaller central defect or thinner glass struts play a similar role in pushing the attenuation to a shorter wavelength. Although these variations, for example the use of a larger central defect, can reduce the attenuation at a specific frequency, they are not effective for other frequencies and would not greatly affect the overall magnitude of the attenuation in a whole transmission window.

Our investigation shows that the most of the confinement loss comes from the coupling between the fundamental mode and the cladding modes situated in the glass layers closest to the central air defect. To effectively reduce the attenuation of the fundamental mode in Kagome-like PCFs, an optimised design of the core-surround is important. A suppressed mode coupling may be achieved by modulating the field profile of the fundamental mode across the glass strips nearest to the central defect. This understanding also provides theoretical support for the recent experiment in a Kagome PCF with a hypocycloid shaped air core [13], for which the attenuation is significantly lower than that in a standard Kagome PCF with a circular shaped central air defect.

Acknowledgments

We thank John Roberts and Tim Birks for helpful discussions in the course of this work and John Roberts for providing the boundary element code used in the calculations for Fig. 2(a).

#141862 - $15.00 USD Received 27 Jan 2011; accepted 9 Mar 2011; published 25 Mar 2011